International Journal of Design & Nature and Ecodynamics
Vol. 21, No. 1, January, 2026, pp. 271-279
Journal homepage: http://iieta.org/journals/ijdne

Antibacterial Chitosan Nanoparticles Synthesized from *Litopenaeus vannamei* Shrimp Shell Waste via Ionic Gelation

Diana Eka Pratiwi[1], Abdul Wahid Wahab[1*], Yusafir Hala[1], Hasri[2], Suriati Eka Putri[2]

[1] Department of Chemistry, Faculty of Mathematics and Natural Science, Hasanuddin University, Makassar 90245, Indonesia
[2] Department of Chemistry, Faculty of Mathematics and Natural Science, Universitas Negeri Makassar, Makassar 90244, Indonesia

Corresponding Author Email: wahidwahab@unhas.ac.id

https://doi.org/10.18280/ijdne.210126

Received: 1 November 2025
Revised: 15 January 2026
Accepted: 23 January 2026
Available online: 31 January 2026

Keywords:
chitosan nanoparticles, shrimp shell, antibacterial

ABSTRACT

The valorization of shrimp shell waste into functional antibacterial materials is a promising strategy to address environmental and health challenges. Herein, chitosan nanoparticles (CS-NPs) were synthesized from whiteleg shrimp shell waste (*Litopenaeus vannamei*) and investigated for their effectiveness against antibiotic-resistant Gram-negative and Gram-positive bacterial species. The ionic gelation method was employed to synthesize CS-NPs by varying the starting chitosan concentration at 0.1, 0.2, 0.3, 0.4, and 0.5% (w/v). Functional group analysis was performed to characterize CS-NPs using an FTIR spectrophotometer, particle size distribution was analyzed using a Particle Size Analyzer (PSA), and morphological characterization was performed using Scanning Electron Microscopy (SEM). CS-NPs displayed a particle size distribution between 29 and 32 nm. SEM analysis indicated that CS-NPS has a smooth surface with no agglomeration. The resulting CS-NPs were then examined for their antibacterial activity. The antimicrobial activity assay toward *Escherichia coli* and *Staphylococcus aureus* revealed that CS-NPs demonstrated remarkable bactericidal activity toward both *E. coli* and *S. aureus*, *d*emonstrating an unusual fourfold enhancement in efficacy toward Gram-negative *E. coli* relative to Gram-positive *S. aureus*. Thus, CS-NPs from white leg shrimp shells represent promising candidates for sustainable antibacterial.

1. INTRODUCTION

Among natural polysaccharides, chitin is the second most widely available after cellulose, and is predominantly contained in the exoskeletons of marine crustaceans and mollusks, as well as in insect cuticles. Among these sources, crustacean waste, particularly white leg shrimp shells, represents the most commonly utilized raw material [1]. Structurally, chitin and chitosan (CS) share similarities with cellulose, as all three polymers consist of long chains of β-(1→4)-linked D-glucose units. In chitin, a group of acetamide occupies the position of C-2 of the glucose unit, whereas in CS this position is substituted by an amine group, forming β-(1→4)-2-amino-2-deoxy-D-glucopyranose. The conversion of chitin to CS occurs through N-deacetylation, during which the acetamide groups in chitin are transformed into amine groups, yielding CS.

Shrimp shell waste accounts for approximately 50–70% of the raw material and contains about 20–30% chitin [2, 3]. The production of CS comprises four main stages: deproteinization, demineralization, decolorization, and deacetylation. Shrimp shells were first deproteinized using a NaOH solution, followed by demineralization with HCl. Decolorization was subsequently carried out using acetone, after which the material was air-dried at ambient temperature to obtain chitin. The chitin was then subjected to deacetylation with NaOH solution to produce CS. Finally, CS was thoroughly washed with running water to attain neutral pH, rinsed with distilled water, filtered, and dried [4]. Whiteleg shrimp (*Litopenaeus vannamei*) is one of the most intensively cultivated shrimp species in Indonesia, particularly in South Sulawesi, generating large quantities of shell waste. Differences in habitat, feed composition, and post-harvest processing may result in compositional variations in shrimp shells, which in turn can affect CS yield and quality. Utilizing locally sourced shrimp shell waste thus provides both scientific insight into source-dependent properties and practical relevance for regional waste management.

CS has been widely applied in multiple industries, such as textiles, agriculture, pharmaceuticals, food, and cosmetics, owing to its distinctive properties such as bioadhesion, biodegradability, biocompatibility, microbial activity, antitumor effects, and tissue-regeneration capability [5-7]. Recently, CS has been engineered into chitosan nanoparticles (CS-NPs), whose reduced particle size leads to significant modifications in physical properties. Compared with bulk CS, CS-NPs exhibit superior characteristics, including nanoscale dimensions, increased surface area, and quantum size effects [8, 9].

Previous studies have described that the bactericidal

efficacy of CS-NPs is largely determined by the source of CS, such as crustacean shells (shrimp or crab) or fungal biomass [9]. Variations in the degree of deacetylation, molecular weight, and residual mineral content result in differences in nanoparticle size, surface charge, and interaction with bacterial cell walls.

CS-NPs are extensively employed as delivery vehicles for drugs, vaccines, and genes [3, 10]. Various methods have been established for CS-NPs fabrication, including cross-linking, ionic gelation, nanoprecipitation, and emulsification [11]. The ionic gelation method offers significant advantages owing to its simplicity, ability to produce small-sized particles, and capacity to encapsulate diverse molecular compounds. CS-NPs are commonly formed through electrostatic interactions between cationic CS and anionic polyanions, such as pectin, sodium tripolyphosphate (TPP), and alginate [12]. Although TPP-mediated ionic gelation is broadly applied for the synthesis of CS-NPs, there is no established universal agreement on the optimum CS/TPP ratio. In general, higher CS concentrations or increased CS:TPP ratios are associated with larger particle sizes and greater tendencies toward agglomeration, whereas excessive TPP concentrations may result in unstable or excessively crosslinked nanoparticle structures [12]. Consequently, determining the suitable concentration of CS and CS-to-TPP ratio requires optimization based on the material source and intended application.

In this study, CS-NPs were produced through the ionic gelation technique by varying the concentration of CS, and then CS-NPs will be used as antibacterial. A number of earlier studies have documented the ability of CS-NPs as antibacterial. Kritchenkov et al. [13] successfully synthesized CS-NPs from commercial CS using the ionic gelation method, showing superior antibacterial efficacy toward *Staphylococcus aureus* and *Escherichia coli* than CS. Furthermore, a similar study was also reported by the previous study, successfully prepared CS-NPs from CS derived from black tiger shrimp shells via the ionic gelation method. The study showed that the synthesized CS-NPs had better bactericidal activity than CS [9]. In this context, the present study focuses on CS-NPs synthesized from whiteleg shrimp shell waste, providing source-specific insights into particle size control and antibacterial activity.

Although CS-NPs been extensively studied, the majority of research utilizes commercially available chitosan or material derived from a limited range of biological sources. The physicochemical properties of CS, including the weight of molecules and the deacetylation degree, are strongly influenced by species origin, environmental factors, and extraction methods. Consequently, source-specific studies are still required to elucidate how locally sourced biomass affects the characteristics and functional performance of CS-NPs. Therefore, this study attempts to synthesize CS-NPs from white leg shrimp shells obtained from waste in South Sulawesi Province, Indonesia, using the ionic gelation method. The synthesized CS-NPs were then used as an antibacterial against *Staphylococcus aureus* and *Escherichia coli* bacteria. From a practical perspective, converting shrimp shell waste into functional CS-NPs offers a low-cost and sustainable alternative to commercially available chitosan-based nanomaterials. This approach supports circular economy principles by transforming abundant local waste into value-added antibacterial products. Moreover, the development of effective antibacterial agents from local biowaste resources is particularly relevant in addressing the increasing prevalence of drug-resistant bacterial infections, especially in regions with limited access to advanced pharmaceutical materials.

2. MATERIALS AND METHOD

2.1 Reagents

CH_3COOH (Merck), NaTPP (PT. Katalis Datesa Prima), Tween 80 (Merck), NaOH (Merck), HCl (Merck), Gram-positive and Gram-negative bacteria were obtained from the Laboratory of Biology Department, Universitas Negeri Makassar, Nutrient Broth (NB) medium, and Nutrient Agar (NA) medium.

2.2 Extraction of chitin and chitosan

The white leg shrimp shell was collected from Makassar, South Sulawesi, Indonesia. White leg shrimp shell waste was thoroughly washed with water to remove attached debris. The sample was dried and mashed, then sieved through a 50-mesh sieve. The CS was extracted from white leg shrimp shells in three stages: demineralization, deproteination, and deacetylation. The demineralization stage was completed with 0.5 M HCl at 90°C for 3 hours, filtration and washing with distilled water were subsequently performed until the pH reached neutrality. Repeated washing with distilled water was performed until a neutral pH of the filtrate was achieved (pH 6.8–7.2). A qualitative $AgNO_3$ test was used as a supplementary confirmation to ensure the absence of residual chloride ions. The residue was dried at 60°C.

The deproteination step was completed with 1 M NaOH, which was refluxed at 65°C for 2 hours prior to washing with distilled water until a neutral pH was attained, and a qualitative test with the addition of acetic acid until no further precipitate was observed. The residue was subsequently dried. Deacetylation was carried out with 50% (w/v) NaOH at 90°C for 1 hour, followed by filtration and subsequent washing with distilled water until a neutral pH was attained [9]. The residue was dried in an oven at 60°C. For more detail the chitin and CS extraction from white leg shrimp shell was shown in Figure 1. Functional group analysis was conducted using an FT-IR spectrophotometer. The KBr pellet method was employed for sample preparation by thoroughly mixing dried CS or CS-NPs with spectroscopic-grade KBr, followed by pressing the mixture into pellets. Spectra were acquired over 4000–400 cm^{-1} at a resolution of 4 cm^{-1}.

2.3 Synthesis CS-NPs

The ionic gelation method was employed for CS-NPs synthesis. CS solutions were dissolved in acetic acid 1% with various concentrations (0.1, 0.2, 0.3, 0.4, and 0.5%) (wt/v), then magnetically stirred for 1 hour at ambient temperature to ensure complete dissolution. This concentration range was selected based on previous reports and preliminary experiments indicating stable nanoparticle formation and minimal agglomeration within this range. Subsequently, an aqueous NaTPP solution (0.1% w/v) was gradually mixed with the CS solution at a fixed volume ratio of CS:TPP = 5:1 under constant magnetic stirring. Tween 80 (0.1% v/v) was added as a stabilizing surfactant agent to minimize nanoparticle agglomeration. The mixture was continuously stirred for 2 h

at ambient temperature to ensure complete ionic crosslinking between anionic phosphate groups of TPP and protonated amine groups of CS. The resulting CS-NPs suspension was freeze-dried.

Polydispersity index (PI) and distribution of particle size were determined by Particle Size Analyzer (PSA). CS-NPs samples were dispersed in distilled water as the dispersion medium and sonicated briefly to prevent aggregation prior to measurement. Measurements were performed at ambient temperature (25°C). The morphology of CS and CS-NPs was examined using Scanning Electron Microscopy (SEM). Prior to observation, Samples were mounted on conductive carbon tape and subsequently sputter-coated with a thin layer of gold to enhance electrical conductivity. SEM imaging was operated at 15 kV with an appropriate working distance.

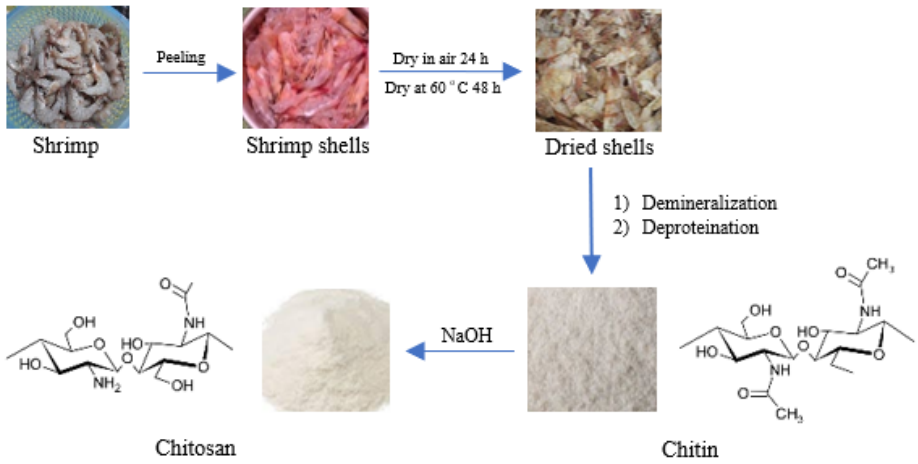

Figure 1. The schematic illustration of chitin and chitosan (CS) extraction from white leg shrimp shell

2.4 Antibacterial activity test

The antimicrobial activity of CS-NPs was assessed using a multi-method approach. The agar well diffusion test was employed for preliminary screening, where diameters of the inhibition zone were measured after a 24 h incubation period. The minimum inhibitory concentration (MIC) was visually assessed using the broth microdilution method, with the lowest concentration showing no turbidity being visually detected as MIC. A CS-NPs stock suspension (defined as 2 mg/mL) was prepared, and serial dilutions were performed by mixing the CS-NPs suspension and NB medium. This procedure produced a series of final CS-NPs concentrations of 0.0316 mg/mL, 0.0636 mg/mL, 0.125 mg/mL, 0.25 mg/mL, 0.5 mg/mL, and 1 mg/mL. Each sample was subsequently inoculated with 1 mL of bacterial suspension adjusted to 1.5×10^8 CFU/mL (0.5 McFarland standard) and incubated at 37°C for 24 h. Subsequently, Minimum Bactericidal Concentration (MBC) was determined by subculturing from clear wells onto Nutrient Agar plates. Bacterial suspensions from MIC test concentrations were serially diluted, spread plated on Nutrient Agar, incubated, and colonies were counted to calculate CFU. The ratio of MBC to MIC was then calculated to classify the antibacterial activity.

3. RESULT AND DISCUSSION

3.1 Chitin and chitosan extraction from white tiger shrimp shell

CS was extracted using a chemical process involving sequential demineralization, deproteination, and deacetylation steps. During the demineralization stage, inorganic minerals such as calcium carbonate and sodium carbonate are converted into their corresponding chloride salts and carbon dioxide, as described in Reaction (1) [14].

$$\begin{aligned} CaCO_3 + 2HCl &\rightarrow CaCl_2 + H_2O + CO_2 \\ Na_2CO_3 + 2HCl &\rightarrow 2NaCl + H_2O + CO_2 \end{aligned} \quad (1)$$

The subsequent step was deproteination, which involves cleaving the bonds between chitin and associated proteins. This stage is particularly critical for CS intended for modification and application in biomedical fields. The chemical reaction occurring during this process is presented in Eq. (2).

$$\begin{aligned} C_6H_{12}N_2O_3 + 2NaOH &\rightarrow 2C_3H_6NNaO_2 \\ C_{10}H_{16}N_2O_7 + 2NaOH &\rightarrow 2C_5H_8NNaO_4 + H_2O \end{aligned} \quad (2)$$

Following the isolation of chitin, a deacetylation process was conducted to obtain CS. In this study, deacetylation was performed using an alkaline treatment method, as illustrated in Eq. (3).

$$C_8H_{15}NO_6 + NaOH \rightarrow C_6H_{13}NO_5 + C_2H_3NaO_2 \quad (3)$$

3.2 Synthesis of chitosan nanoparticles

CS-NPs were prepared by the ionic gelation method through cross-linking of CS with NaTPP. Tween 80, as a neutral surfactant, might reduce the particle size. Tween 80 is a molecule that is absorbed by the particle surface to inhibit agglomeration [15, 16]. Because the presence of surfactants covers and stabilizes the CS particles in the solution, the particle breakdown process is more effective, and agglomeration does not occur. The electrostatic interaction between positively charged CS and negatively charged TPP underlies the production of CS-NPs. With the addition of acetic acid, CS becomes polycationic under acidic conditions.

TPP dissociates in water to generate polyanionic $P_3O_{10}^{5-}$ ions and OH^-, which subsequently electrostatically interact with NH_3^+ groups of CS [12]. Ionotropic gelation between CS and NaTPP is shown in Figure 2.

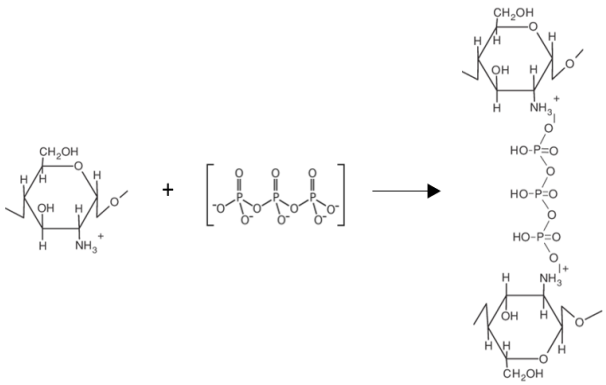

Figure 2. Ionotropic gelation between chitosan (CS) and NaTPP in chitosan nanoparticles (CS-NPs) synthesis

3.3 Functional group of chitosan and chitosan nanoparticles

Determination of functional groups CS and CS-NPs according to analysis results using the FTIR spectrophotometer, shown in Figure 3. The intense and broad absorption band observed in the range of 3500–3200 cm^{-1} aligns with overlapping N–H stretching vibrations of hydroxyl and amino groups and O–H stretching, indicating extensive intermolecular hydrogen bonding in CS. Similar stretching vibrations of N–H bonds in primary and secondary amines were observed overlapping with the O–H region in the range of 3400–3200 cm^{-1} have been previously reported [17, 18]. Absorption of CS-NPs was indicated by the shift in $-NH_2$ and OH peak position and shape, as the amine groups become protonated (NH_3^+) to interact ionically with the TPP croslinker.

Sharp and weak-to-medium peaks within 2950-2870 cm^{-1} are attributed to the C-H bond. Since the C-H bonds are not directly involved in the ionic cross-linking reaction, the position and intensity of the peaks remain relatively constant in CS and all CS-NPs spectra. The absorption band around 1650 cm^{-1} can be attributed to the amide I band, which mainly originates from C=O stretching vibrations of remaining N-acetylated groups. Meanwhile, the band near 1590 cm^{-1} corresponds to the amide II band, associated with coupled N–H bending and C–N stretching vibrations of the amino groups. In CS-NPs, the relative intensity of the amide I and amide II absorption bands decreases, indicating protonation of $–NH_2$ groups ($–NH_3^+$) and their involvement in ionic interactions with TPP. This interaction was further confirmed by the lower intensity of the amide band in CS-NPs compared to CS [19].

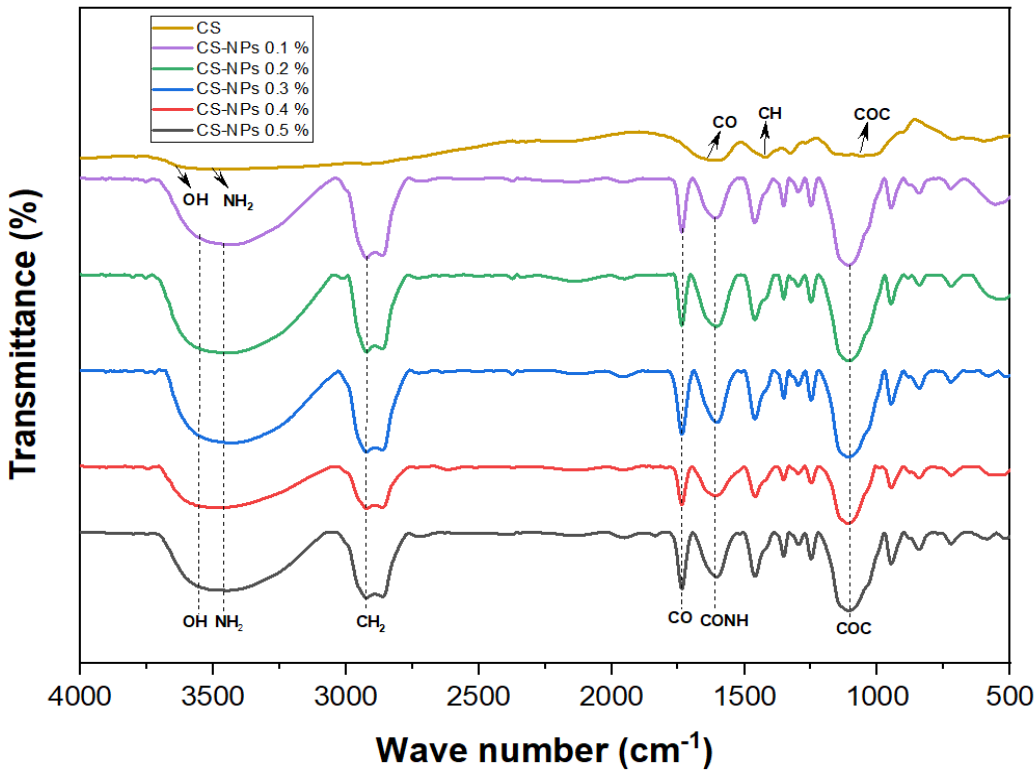

Figure 3. FTIR spectra of chitosan (CS) and chitosan nanoparticles (CS-NPs) prepared at varying initial chitosan concentrations

Moreover, the weak-to-medium absorption bands observed at 2950–2870 cm^{-1} correspond to aliphatic C–H (–CH and $–CH_2$) stretching vibrations, which remain relatively unchanged after nanoparticle formation, as these bonds are not directly involved in the ionic gelation process. Notably, new absorption bands appear in the range of 1250–1200 cm^{-1} and 1100–900 cm^{-1} in the CS-NPs spectra, which correspond to P–O and P=O stretching vibrations of the $P_3O_{10}^{5-}$ ion from TPP. The emergence of these phosphate-related bands, together with the modification of $–NH_3^+$-related peaks, provides clear evidence of TPP-mediated ionic cross-linking of CS during CS-NPs formation. These spectral features provide combined evidence for the successful formation of CS-NPs through ionotropic gelation arising from electrostatic attraction of

protonated amine ($–NH_3^+$) groups of CS and $P_3O_{10}^{5-}$ anions of TPP [20]. The formation of CS-NPs via TPP crosslinking is consistent with previous findings [9, 16]. Additionally, the broad region at 1150–1020 cm^{-1} can be attributed to C–O–C stretching vibrations of the polysaccharide backbone, which partially overlap with P–O vibrations in CS-NPs, further supporting the formation of CS–TPP nanoparticles.

3.4 Particle size of CS-NPS

The particle size distribution of CS-NPs was determined using PSA. The obtained results are presented in Figure 4 and Table 1. In addition to providing the average particle size, PSA also yields the PI, indicating the uniformity of distribution of particle size. A PI value below 0.5 suggests a relatively homogeneous particle population, whereas a PI value above 0.5 signifies a highly heterogeneous distribution. Similar PI values for CS-NPs have been reported in previous studies [3].

The average particle size of CS-NPs showed an increasing trend as the initial CS concentration increased. Specifically, CS-NPs synthesized using CS concentrations of 0.1, 0.2, 0.3, 0.4, and 0.5% (w/v) exhibited average particle sizes of 29.2, 30.5, 32.5, 32.4, and 32.4 nm, respectively (Table 1). Overall, particle sizes were in the range of 29 to 32 nm across the studied concentration range.

The particle size of CS-NPs exhibited a gradual increase with higher initial CS concentrations, rising from 29.2 nm at 0.1% (w/v) to 32.4 nm at 0.5% (w/v). Notably, the associated PI values remained low, ranging from 0.215 to 0.395, which indicates a relatively narrow and uniform particle size distribution. Consequently, the increase in particle size is unlikely to result from particle agglomeration. Rather, this pattern can be ascribed to the greater availability of CS molecular chains at higher concentrations, which facilitates the formation of a denser and more extensive crosslinked network during ionic gelation with TPP. With an increasing number of protonated amino groups ($–NH_3^+$) that engage in electrostatic interactions with TPP, the nanoparticles increase in size while preserving good monodispersity.

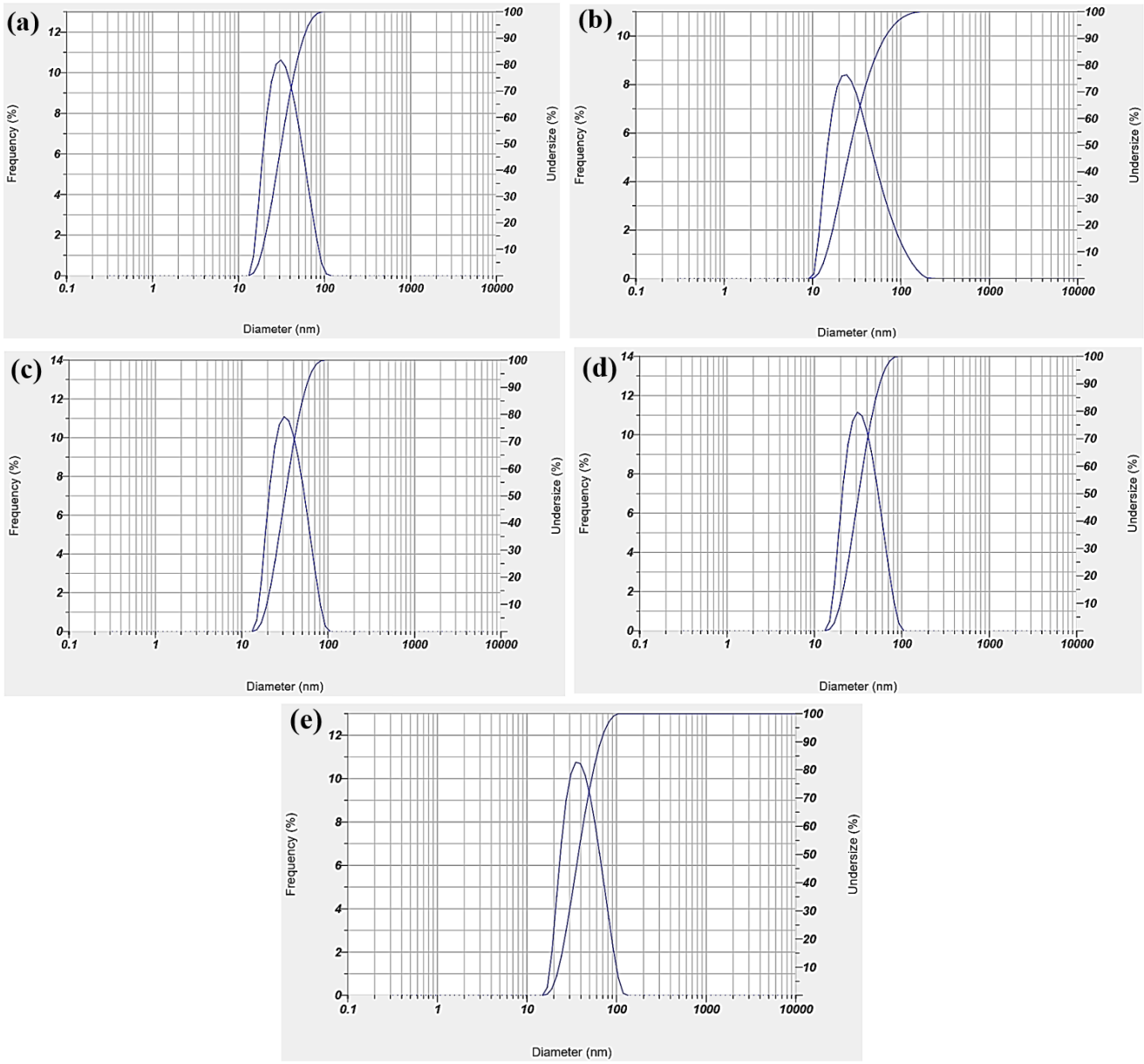

Figure 4. Particle size distribution of (a) CS-NPs 0.1%, (b) CS-NPs 0.2%, (c) CS-NPs 0.3%, (d) CS-NPs 0.4%, (e) CS-NPs 0.5%

Table 1. Particle size and Polydispersity Index value correspond to Figure 4

Sample	The Average Particle Size (nm)	Polydispersity Index (PI)
CS-NPs 0.1%	29.2	0.395
CS-NPs 0.2%	30.5	0.335
CS-NPs 0.3%	32.5	0.257
CS-NPs 0.4%	32.4	0.215
CS-NPs 0.5%	32.4	0.293

The results achieved are consistent with the previous study. Similarly, Nguyen et al. [2] examined the effect of varying initial CS concentration (0.3 to 2.1%) and the particle size distribution of CS-NPs increase by the increasing of initial CS concentration, yielding particle sizes in the range of 735.9–1441.7 nm. The similar phenomena were also reported by the previous study, which varied the similar initial CS concentration of 0.1 to 0.5%, exhibiting an average particle size of 92.89 nm to 407.0 nm using CS extracted from black tiger shrimp shell with the same method [9]. It indicates that the CS-NPs from white leg shrimp shell produces the smaller average particle size.

3.5 Morphology of chitosan and chitosan nanoparticles

Morphological characterization of the samples was performed using SEM, as presented in Figure 5. Pristine CS showed irregular, rough, and agglomerated structures, which are characteristic of bulk CS powder. In contrast, the CS-NPs exhibited well-defined nanoscale morphologies that varied according to the initial CS concentration. The localized clustering evident in the SEM micrographs is likely due to the sample drying procedure and does not necessarily indicate aggregation in aqueous dispersion.

At lower CS concentrations (0.1–0.2%), CS-NPs exhibited relatively discrete, bead-like or dendritic structures. As the CS concentration increased (0.3–0.5%), the particles tended to form clustered assemblies with less uniform morphology. This apparent aggregation is likely associated with increased interparticle interactions during solvent evaporation and freeze-drying prior to SEM observation.

It should be noted that SEM images represent the morphology of dried samples under high vacuum conditions. Therefore, the observed particle clustering does not necessarily reflect aggregation in aqueous dispersion. This interpretation is supported by the low PI values obtained from PSA analysis, which indicate relatively homogeneous particle size distributions in suspension.

The dendrimer morphology of the sample was identified in the CS-NPs 0.2%, while the bead morphology was identified in the CS-NPs 0.1% and CS-NPs 0.4% samples. The morphological structure of the CS-NPs sample is larger than that of CS-NPs 0.4%, indicating the occurrence of agglomeration, which is in line with the average particle size in Table 1. An anomaly is shown in the CS-NPs 0.4% and CS-NPs 0.5% samples; both have the same average particle size but show very different morphologies. It is expected because the PI value in the CS-NPs 0.5% sample is very high (Table 1), so that the morphology shown is not homogeneous with a smooth surface. Previous studies on CS-NPs synthesized from black tiger shrimp shells reported similar morphologies [9]. Thus, PSA and SEM results are complementary, where PSA reflects particle behavior in dispersion, while SEM reveals structural organization in the dried state.

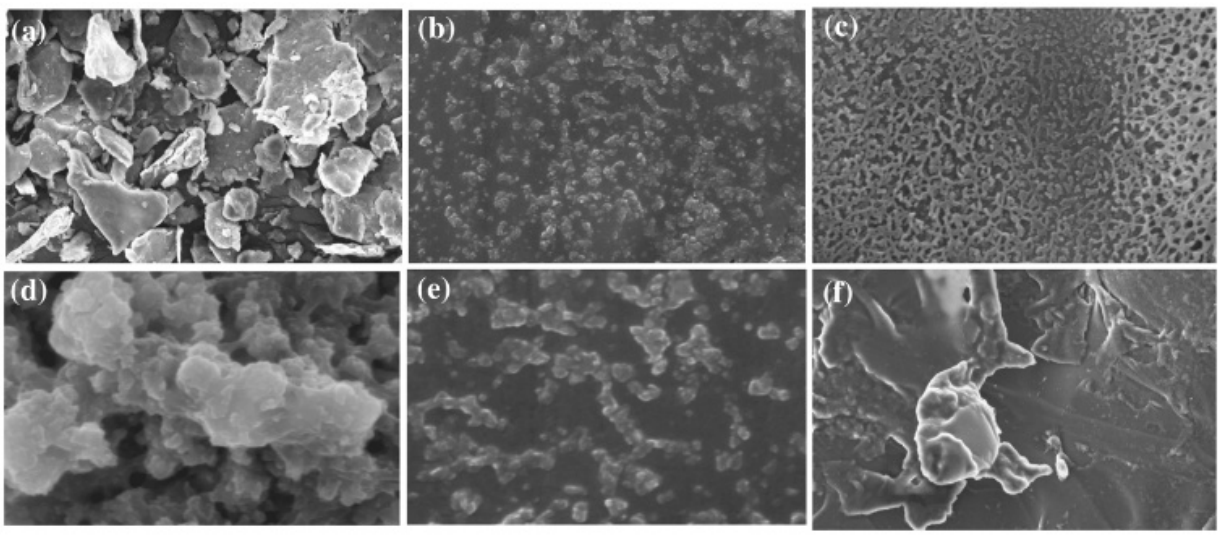

Figure 5. Morphology of (a) CS, (b) CS-NPs 0.1%, (c) CS-NPs 0.2%, (d) CS-NPs 0.3%, (e) CS-NPs 0.4%, (f) CS-NPs 0.5%, using SEM at 15 kV

3.6 Antibacterial activity of CS-NPs

The microbial activity of CS-NPs is shown in Figure 6. The CS-NPs exhibited weak to moderate microbial activity with a diameter of inhibition zones of 13.67 mm toward *S. aureus* and 9.25 mm toward *E. coli*. These values were significantly smaller than the positive control (tetracyclin), which has a diameter of inhibition zone of 22.472 mm toward *S. aureus* and 16.295 mm toward *E. coli*, suggesting limited diffusion or lower potency of CS-NPs under the tested conditions. This is in line with the previous study, which also examined the microbial test of CS-NPs toward *S. aureus* and *E. coli* [21].

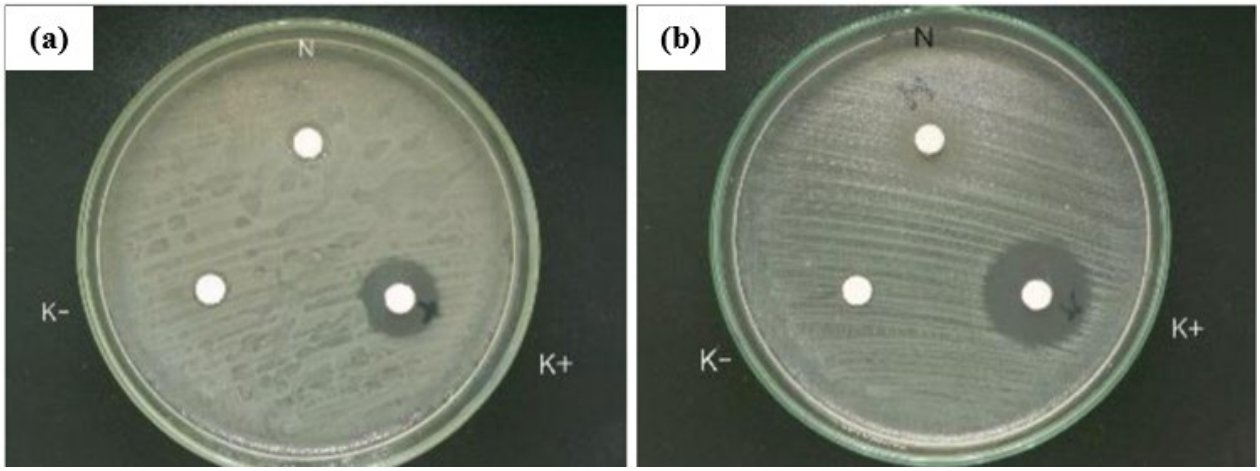

Figure 6. Antibacterial test of CS-NPs toward (a) *E. coli* and (b) *S. aureus*

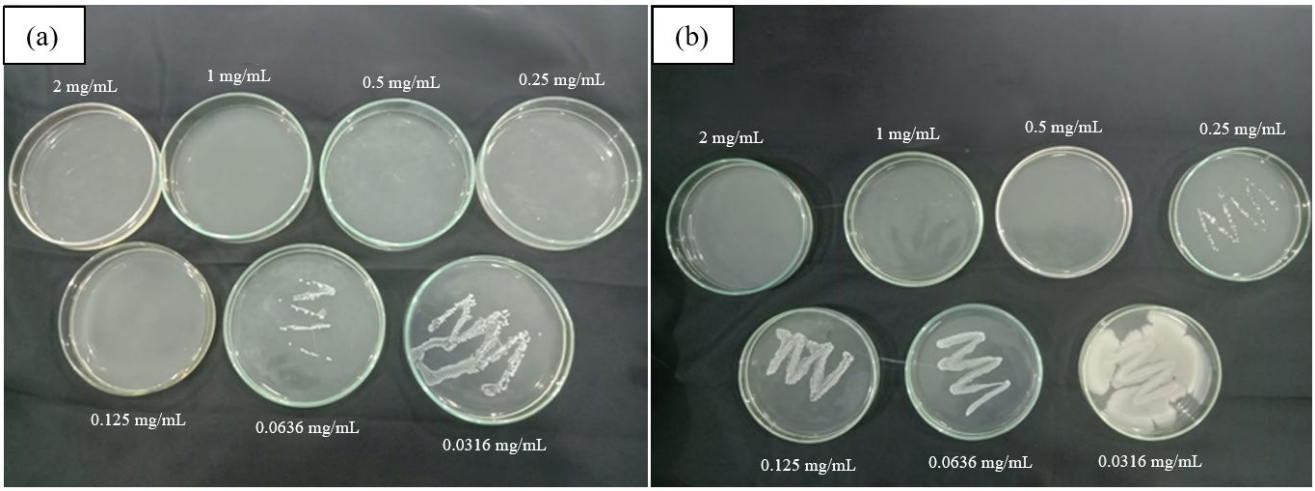

Figure 7. MBC test of CS-NPs toward (a) *E. coli* and (b) *S. aureus*

Table 2. Minimum inhibitory concentration (MIC) of CS-NPs toward *S. aureus* and *E. coli*

Concentration of CS-NPs (mg/mL)	*S. aureus*	*E. coli*
0.0316	+	+
0.0636	+	-
0.125	+	-
0.25	-	-
0.5	-	-
1	-	-
2	-	-

Note: A positive result (+), observed as turbidity or cloudiness in the solution, indicates active bacterial growth. Conversely, a negative result (-), observed as a clear solution, indicates that bacterial growth has been inhibited.

MIC values of CS-NPs toward *Escherichia coli* and *Staphylococcus aureus* were determined via turbidimetric analysis (Table 2). Minimum growth inhibition was observed at 0.25 mg/mL for S. aureus and 0.0636 mg/mL for *E. coli*.

The observed disparity, where CS-NPs exhibit a larger inhibition zone toward *S. aureus* yet a lower MIC toward *E. coli,* is not an anomaly but a documented phenomenon for nanoparticle-based antimicrobials [22, 23]. This observation can be explained by two key factors: the method-dependent diffusibility of nanoparticles in solid agar versus liquid broth [24, 25], and the differential interaction mechanisms with Gram-positive and Gram-negative cell envelopes [26, 27]. The agar diffusion assay, influenced by particle size and agar interaction, may favor the presentation of activity toward *S. aureus*, whose porous peptidoglycan layer may trap nanoparticles, creating a larger zone. In contrast, the broth microdilution method, which ensures direct contact, reveals the superior membrane-disrupting potency of cationic CS-NPs toward the outer membrane with a high negative charge density of *E. coli*, resulting in lower MIC values [28].

The MBC test of CS-NPs toward *E. coli* and *S. aureus* is shown in Figure 7. The quantitative microbial activity of the synthesized CS-NPs was assessed and summarized in Table 3.

Table 3. MIC, MBC, and MBC/MIC ratio values of CS-NPs

Parameters	*S. aureus*	*E. coli*
MIC	0.25 mg/mL	0.0636 mg/mL
MBC	0.5 mg/mL	0.125 mg/mL
MBC/MIC ratio	2	1.97

The differential MBC values (0.125 mg/mL for *E. coli* vs. 0.5 mg/mL for *S. aureus*) robustly demonstrate that the Gram-negative bacteria *E. coli* present greater susceptibility to the bactericidal action of CS-NPs under the tested conditions. This phenomenon is mainly ascribed to high-affinity electrostatic attraction of cationic CS-NPs and the anionic lipopolysaccharide (LPS) layer of *E. coli*, leading to efficient outer membrane disruption, followed by damage to underlying structures. The thick, absorptive peptidoglycan layer of *S.*

aureus provides a more significant physical and electrostatic barrier, necessitating a higher concentration to achieve equivalent lethal damage. These findings align with the general trend observed for many cationic antimicrobial polymers and peptides, highlighting the critical role of initial cell surface interaction in determining antibacterial efficacy, as previously reported by research [22, 28]. These findings position the synthesized CS-NPs as particularly promising for combating problematic Gram-negative infections and warrant investigation into their mechanism and potential against multidrug-resistant strains.

The consistent MBC/MIC ratio of approximately 2 for both bacterial strains indicates concentration-dependent bactericidal activity with a narrow window between inhibition and killing. This ratio, significantly below the 4-fold cutoff for bactericidal classification, demonstrates that a mere doubling of concentration above the MIC is sufficient to achieve ≥ 99.9% bacterial eradication. This aligns with the fundamental pharmacodynamic principle that bactericidal agents kill pathogens, a property distinct from mere growth inhibition. The result obtained is in accordance with previous findings [29, 30]. The consistency across phylogenetically distinct bacteria (both Gram-positive *S. aureus* and Gram-negative *E. coli*) further suggests a common lethal mechanism, likely through rapid and irreversible membrane disruption facilitated by the CS-NPs' nanoscale dimensions and high positive charge density.

4. CONCLUSION

The particle size of the CS-NPs showed a significant increase from 29.2 nm to 32.4 nm with an increase in the initial concentration of CS from 0.1% to 0.5%, which is attributed to enhanced crosslinking and polymer chain availability. Although SEM images show apparent aggregation, this may be attributed to drying effects during sample preparation, as indicated by low PI values confirming good dispersion in suspension. The resulting CS-NPs were then examined for their antibacterial activity. The microbial activity assay toward *Escherichia coli* and *Staphylococcus aureus* revealed that CS-NPs were more active in inhibiting Gram-negative bacteria (*E. coli*) than Gram-positive bacteria (*S. aureus*). Therefore, CS-NPs from white leg shrimp shells can be developed for antibacterial use in human daily life. Despite the promising antibacterial activity observed, certain limitations of this study merit acknowledgment. The antibacterial mechanism of CS-NPs was inferred based on existing literature and was not experimentally investigated. In addition, cytotoxicity assessment toward mammalian cells was not conducted, which is essential for evaluating potential biomedical applications. Future studies should focus on elucidating the antibacterial mechanism, evaluating cytotoxicity and biocompatibility, expanding antibacterial tests to a broader range of clinically relevant bacteria, and assessing the long-term physicochemical stability of CS-NPs to support their practical application.

ACKNOWLEDGEMENTS

The authors gratefully acknowledge the Ministry of Education, Culture, Research, and Technology for financial support through the Doctoral Dissertation Research Fund (PDD Grant), Contract No. 12688/UN4.22/PT.01.03/2022.

REFERENCES

[1] Chen, W., Cheng, H., Chen, L., Zhan, X., Xia, W. (2021). Synthesis, characterization, and anti-tumor properties of O-benzoylselenoglycolic chitosan. International Journal of Biological Macromolecules, 193: 491-499. https://doi.org/10.1016/j.ijbiomac.2021.10.086

[2] Nguyen, T.D., Pham, Q.T., Nguyen, K.K., Nguyen, T.N. (2024). Stability study and antifungal activity of chitosan films from shrimp shells against Colletotrichum gloeosporioides. Tropical Journal of Natural Product Research, 8(6): 7345-7349. https://doi.org/10.26538/tjnpr/v8i6.2

[3] Koirala, P., Bhandari, Y., Khadka, A., Kumar, S.R., Nirmal, N.P. (2024). Nanochitosan from crustacean and mollusk byproduct: Extraction, characterization, and applications in the food industry. International Journal of Biological Macromolecules, 262: 130008. https://doi.org/10.1016/j.ijbiomac.2024.130008

[4] Bui-Phuc, T., Dinh-Phong, N., Thai-Hoang, L., Anh-Dao, L.T., Cong-Hau, N. (2023). Preparation of antibacterial chitosan membrane and potential application as coating in maintaining the quality of jackfruit. Tropical Journal of Natural Product Research, 7(9): 4059-4064. https://doi.org/10.26538/tjnpr/v7i9.32

[5] Mawazi, S.M., Kumar, M., Ahmad, N., Ge, Y., Mahmood, S. (2024). Recent applications of chitosan and its derivatives in antibacterial, anticancer, wound healing, and tissue engineering fields. Polymers, 16(10): 1351. https://doi.org/10.3390/polym16101351

[6] Yadav, M., Kaushik, B., Rao, G.K., Srivastava, C.M., Vaya, D. (2023). Advances and challenges in the use of chitosan and its derivatives in biomedical fields: A review. Carbohydrate Polymer Technologies and Applications, 5: 100323. https://doi.org/10.1016/j.carpta.2023.100323

[7] Yang, J., Lu, H., Li, M., Liu, J., Zhang, S., Xiong, L., Sun, Q. (2017). Development of chitosan-sodium phytate nanoparticles as a potent antibacterial agent. Carbohydrate Polymers, 178: 311-321. https://doi.org/10.1016/j.carbpol.2017.09.053

[8] Darwesh, O.M., Sultan, Y.Y., Seif, M.M., Marrez, D.A. (2018). Bio-evaluation of crustacean and fungal nano-chitosan for applying as food ingredient. Toxicology Reports, 5: 348-356. https://doi.org/10.1016/j.toxrep.2018.03.002

[9] Putri, S.E., Ahmad, A., Raya, I., Tjahjanto, R.T., Irfandi, R. (2023). Synthesis and antibacterial activity of chitosan nanoparticles from black tiger shrimp shell (Penaeus monodon). Egyptian Journal of Chemistry, 66(8): 129-139.

[10] Elumalai, S., Somasundaram, A., Ramasamy, P. (2025). A comprehensive review on nanochitosan and its diverse applications in various industries. International Journal of Biological Macromolecules, 305: 141150. https://doi.org/10.1016/j.ijbiomac.2025.141150

[11] Yanat, M., Schroën, K. (2021). Preparation methods and applications of chitosan nanoparticles; with an outlook toward reinforcement of biodegradable packaging. Reactive and Functional Polymers, 161: 104849. https://doi.org/10.1016/j.reactfunctpolym.2021.104849

[12] Hoang, N.H., Le Thanh, T., Sangpueak, R., Treekoon, J., Saengchan, C., Thepbandit, W., Buensanteai, N. (2022). Chitosan nanoparticles-based ionic gelation method: A promising candidate for plant disease management. Polymers, 14(4): 662. https://doi.org/10.3390/polym14040662

[13] Kritchenkov, A.S., Kurasova, M.N., Godzishevskaya, A.A., Mitrofanova, E.S., Egorov, A.R., Yagafarov, N.Z., Khrustalev, V.N. (2021). High antibacterial activity and low toxicity of pyridoxal derivatives of chitosan and their nanoparticles. Mendeleev Communications, 31(4): 504-506. https://doi.org/10.1016/j.mencom.2021.07.022

[14] Benhabiles, M.S., Salah, R., Lounici, H., Drouiche, N., Goosen, M.F.A., Mameri, N. (2012). Antibacterial activity of chitin, chitosan and its oligomers prepared from shrimp shell waste. Food Hydrocolloids, 29(1): 48-56. https://doi.org/10.1016/j.foodhyd.2012.02.013

[15] Arifin, M.F., Shafira, E., Noviani, Y., Desmiaty, Y., Okta, F.N. (2024). Nanosuspension formula of Curcuma Xanthorriza rhizome dry extract: Impact of tween 80-PEG 400 ratio. Sciences of Pharmacy, 3(2): 112-119. https://doi.org/10.58920/sciphar0302222

[16] Hasri, Pratiwi, D.E., Putri, S.E., Alimin. (2019). Adsorption study for removal of acid orange dye using modified nano chitosan. Journal of Physics: Conference Series, 1244(1): 012034. https://doi.org/10.1088/1742-6596/1244/1/012034

[17] Ramanery, F.P., Mansur, A.A., Mansur, H.S. (2013). One-step colloidal synthesis of biocompatible water-soluble ZnS quantum dot/chitosan nanoconjugates. Nanoscale Research Letters, 8(1): 512. https://doi.org/10.1186/1556-276X-8-512

[18] Zam, Z.Z., Muin, F., Fataruba, A. (2021). Identification of chitosan beads from coconut crab patani variety using Fourier Transform Infrared Spectroscopy (FTIR). Journal of Physics: Conference Series, 1832(1): 012014. https://doi.org/10.1088/1742-6596/1832/1/012014

[19] Hamedi, H., Moradi, S., Hudson, S.M., Tonelli, A.E. (2018). Chitosan based hydrogels and their applications for drug delivery in wound dressings: A review. Carbohydrate Polymers, 199: 445-460. https://doi.org/10.1016/j.carbpol.2018.06.114

[20] Laosinwattana, C., Somala, N., Dimak, J., Teerarak, M., Chotsaeng, N. (2025). Ultrasonic emulsification of Cananga odorata nanoemulsion formulation for enhancement of herbicidal potential. Scientific Reports, 15(1): 3263. https://doi.org/10.1038/s41598-025-87810-1

[21] Yadav, P., Yadav, A.B., Gaur, P., Mishra, V., Huma, Z.I., Sharma, N., Son, Y.O. (2022). Bioengineered ciprofloxacin-loaded chitosan nanoparticles for the treatment of bovine mastitis. Biomedicines, 10(12): 3282. ttps://doi.org/10.3390/biomedicines10123282

[22] Das, B., Dash, S.K., Mandal, D., Ghosh, T., Chattopadhyay, S., Tripathy, S., Roy, S. (2017). Green synthesized silver nanoparticles destroy multidrug resistant bacteria via reactive oxygen species mediated membrane damage. Arabian Journal of Chemistry, 10(6): 862-876. https://doi.org/10.1016/j.arabjc.2015.08.008

[23] Chung, E., Ren, G., Johnston, I., Matharu, R.K., Ciric, L., Walecka, A., Cheong, Y.K. (2023). Applied methods to assess the antimicrobial activity of metallic-based nanoparticles. Bioengineering, 10(11): 1259. https://doi.org/10.3390/bioengineering10111259

[24] Zhang, X., Hou, X., Ma, L., Shi, Y., Zhang, D., Qu, K. (2023). Analytical methods for assessing antimicrobial activity of nanomaterials in complex media: Advances, challenges, and perspectives. Journal of Nanobiotechnology, 21(1): 97. https://doi.org/10.1186/s12951-023-01851-0

[25] Punz, B., Christ, C., Waldl, A., Li, S., et al. (2025). Nano-scaled advanced materials for antimicrobial applications-mechanistic insight, functional performance measures, and potential towards sustainability and circularity. Environmental Science: Nano, 12(3): 1710-1739. https://doi:10.1039/D4EN00798K

[26] Wang, L., Hu, C., Shao, L. (2017). The antimicrobial activity of nanoparticles: Present situation and prospects for the future. International Journal of Nanomedicine, 12: 1227-1249. https://doi.org/10.2147/IJN.S121956

[27] More, P.R., Pandit, S., Filippis, A.D., Franci, G., Mijakovic, I., Galdiero, M. (2023). Silver nanoparticles: Bactericidal and mechanistic approach against drug resistant pathogens. Microorganisms, 11(2): 369. https://doi.org/10.3390/microorganisms11020369

[28] Hochvaldová, L., Panáček, D., Válková, L., Večeřová, R., Kolář, M., Prucek, R., Panáček, A. (2024). *E. coli* and *S. aureus* resist silver nanoparticles via an identical mechanism, but through different pathways. Communications Biology, 7(1): 1552. https://doi.org/10.1038/s42003-024-07266-3

[29] Ishak, A., Mazonakis, N., Spernovasilis, N., Akinosoglou, K., Tsioutis, C. (2025). Bactericidal versus bacteriostatic antibacterials: Clinical significance, differences and synergistic potential in clinical practice. Journal of Antimicrobial Chemotherapy, 80(1): 1-17. https://doi.org/10.1093/jac/dkae380

[30] Batista, S., Fernandez-Pittol, M., San Nicolás, L., Martínez, D., Narváez, S., Espasa, M., González-Martin, J. (2025). Design and validation of a simplified method to determine minimum bactericidal concentration in nontuberculous mycobacteria. Antibiotics, 14(4): 381. https://doi.org/10.3390/antibiotics14040381